

A parameterized Geometry Interpolation Method for Human Body Modeling

Dirk Fressmann¹, Anja Wagner², Steffen Peldschus³, Andre Eggers⁴

¹DYNAmore GmbH

²Ludwig-Maximilians University Munich

³Hochschule Furtwangen University

⁴Bundesanstalt für Strassenwesen (BASt)

1 Introduction and Problem Description

Human body modeling has become very important in the automotive industry within the last couple of years. One issue with human models is that most of the well-known models, like for instance the THUMS™ models (Toyota Motor Corporation [1]-[3]) or the GHBM models [4] are only available in standardized sizes and postures, e.g. 50/95%ile male, 5%ile female or 6 year-old child among others. However, real human bodies vary in size, geometry and stiffness distribution (cf. Figure 1). Therefore, worst-case scenarios are often aspired, where the size and shape of the human body is chosen, such that the model behavior in a crash test scenario leads to extreme responses in terms of injury criteria or the interaction with the vehicle. These worst-case geometries of the human body are usually obtained by using different body sizes (e.g. 6 year-old child, 5%ile female or 95%ile male). However the shape of the body also has a tremendous influence and is hardly accounted for. Examples for different body shapes are for instance skinny or obese shapes or changes due to ageing effects. Since the worst-case geometries are not known in advance, various simulations have to be performed for each crash test scenario to study the behavior of different body shapes. This of course requires a fast and reliable method for modifying the human body model, according to specific parameters to modify e.g. the shape of the thorax or the abdomen, the size of the extremities or the posture of the human body.

This paper describes a method, where the shape of the human body can easily be modified using specific parameters or the motion of control points. The shape of the body – as described by the nodal coordinates of the FE mesh – is then obtained by a non-linear, multi-step interpolation approach of the remaining model nodes.

Examples will be demonstrated using the THUMS™ human body, developed by Toyota Motor Corporation and Toyota Central R&D Labs Inc. approximately since 2000. The THUMS™ represents a model of the human body which is primarily used in automotive crash test scenarios. Further information can be found in the references [1]-[3].



Figure 1: Multiple shapes of the human body (reprinted from B. Allen et al., The space of human body shapes: Reconstruction and parameterization from range scans, University of Washington, 2003)

1.1 Problem Description

Multiple reasons for the need to change the body shape are possible, like the fitness level of the subject, the general size or changes related to ageing, where the latter case should be focused on in this paper. Increasing age especially leads to a change of the thoracic geometry. This mainly includes

the increase of the rib inclination angle or the curvature of the spine. The change of the rib angle leads to an increased depth of the thorax in the anterior-posterior direction together with a changing mechanical behavior of the rib cage (cf. Figure 2). In case of a frontal impact, the ribs in the younger ribcage will mainly rotate around the spine connection due to the steep rib angle, while the older ribcage will sustain increased straining of the ribs and thus an increased probability for possible rib fractures is present.

The evaluation of the CT scan database led to the insight that the geometry of the current THUMS 3 models represents a rather young individual and a geometrical adaptation of the full model is necessary to represent the older population. Note that a crucial requirement for any geometric modification procedure is that the model and mesh quality after such an adaptation process has to be in a good condition for the actual crash phase.

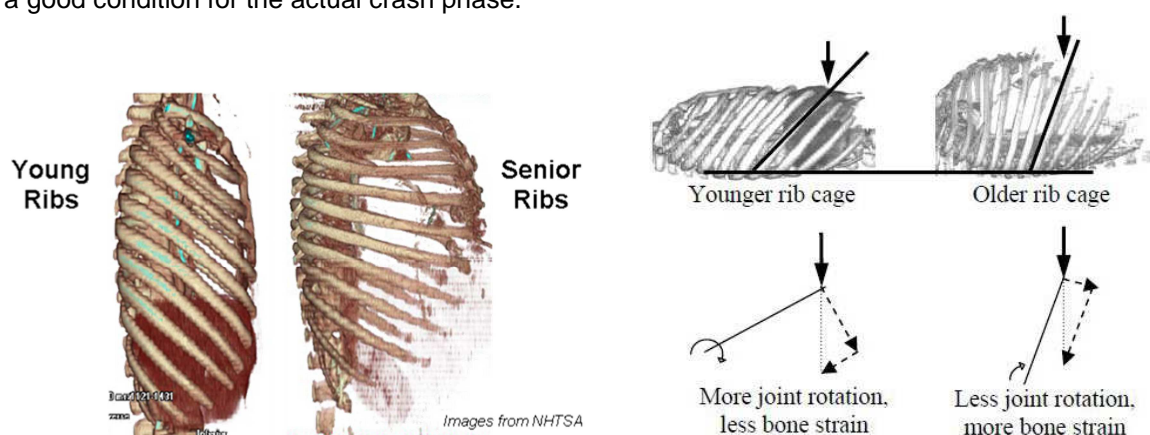


Figure 2: (left) comparison of a "young" rib cage and an "old" rib cage, (right) different load distribution, depending on the inclination angle in a frontal impact situation

1.2 Data Capturing and Geometric Interpolation

Data from CT scans cannot be directly used in finite element analyses. Either three dimensional volumes have to be generated and correspondingly meshed to obtain a new FE model or the geometry of an available human model has to be adapted, based on the CT scan geometry. Especially the latter case requires a parameterization of the CT thorax geometry. This can be achieved in terms of anatomical landmarks or control points, which are distributed over the whole thorax geometry (rib cage, cf. Figure 3). A new geometry might then be obtained by defining motion vectors for the landmarks on the FE mesh or by mapping two different sets of landmarks onto each other, i.e. defining a relation between the landmarks of the CT-based geometry and of the FE mesh.

This approach can conveniently be used for an interpolation process of the whole FE geometry, represented by the nodal coordinates of the mesh. The landmarks are taken as control points for the interpolation, where the locations are available on the initial mesh and on the new thorax. This data can then be used to setup an interpolation process for the remaining nodes of the surrounding flesh, the bones and the organs, which will be described in the following.

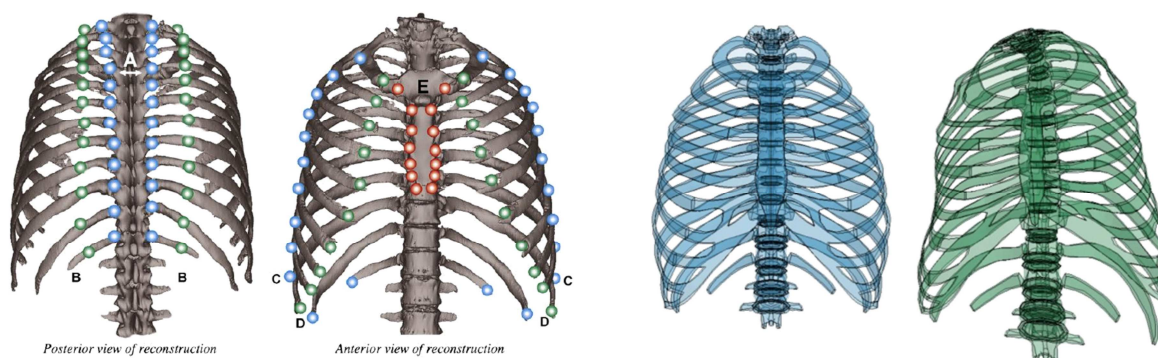


Figure 3: (left) example for a specific distribution of landmarks, (right) initial and deformed THUMS V3 thorax geometry (example)

2 Geometry Interpolation Method

2.1 The Mathematical Problem

For the geometrical adaptation of the mesh, we choose an interpolation method in favor of a least-squares approximation. While in the latter approach the control points are only approximated, depending on the type of the least squares formulation, the interpolation method matches the control points exactly. Thus we seek a control-point-based interpolation method for multi-dimensional data with exact fit of the data points.

Given is a set of N data points, representing the landmarks/control points \mathbf{x}_j , where $j=1, \dots, N$ and corresponding data values $f(\mathbf{x}_j)$. The interpolation function can then be written as

$$s(\mathbf{x}) = \sum_{j=1}^N \lambda_j \psi_j(\mathbf{x}) \quad (1)$$

with the interpolation weights λ_j and the interpolation function $\psi_j(\mathbf{x})$. The matching of the control points requires that the equation $s(\mathbf{x}_j) = f(\mathbf{x}_j)$ is fulfilled and the evaluation of the interpolation function at the control points reflects the corresponding data values.

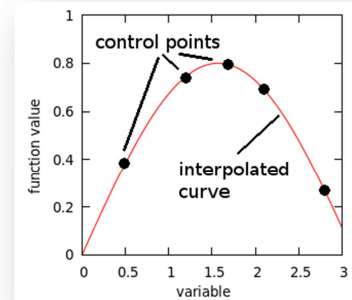


Figure 4: interpolation of a curve based on 5 control points

Special Case Example: In case of a linear interpolation approach, the well-known N_1 shape functions used in finite element analyses or standard morphing approaches are obtained, where each point in space is interpolated linearly using the motion or location of the vertices of the finite element or the morphing box. This linear approach leads to very limited approximation possibilities and large local deformations cannot be realized. For this reason, FE meshes or morphing regions have to be refined or replaced by higher-order shape functions.

Therefore, nonlinear interpolation functions are used in this case, where especially two approaches are considered, namely a *radial basis function* approach and the *kriging* approach, which are explained in more detail in the following.

2.1.1 Radial Basis Function (RBF) Approach

A radial basis function ϕ is a real-valued, radially symmetric function which only depends on the distance of a given point from a reference, i.e. $\phi(r_j) \geq 0$, with $r_j = \|\mathbf{x} - \mathbf{x}_j\|$. Therefore, ψ_j is replaced by $\phi(r_j)$ in Eq. (1). Additionally, Eq. (1) is augmented by a polynomial term such that

$$s(\mathbf{x}) = \sum_{j=1}^N \lambda_j \phi(r_j) + \sum_{k=1}^M \gamma_k p_k(\mathbf{x}) \quad (2)$$

where p_k is chosen to be a polynomial of degree $k-1$ and γ_k are the corresponding weights. The latter, polynomial term ensures a positive definite matrix and thus a unique solution of the system. This finally leads to the symmetric linear equation system

$$\begin{bmatrix} \mathbf{A} & \mathbf{P} \\ \mathbf{P}^T & \mathbf{0} \end{bmatrix} \begin{bmatrix} \boldsymbol{\lambda} \\ \boldsymbol{\gamma} \end{bmatrix} = \begin{bmatrix} \mathbf{f} \\ \mathbf{0} \end{bmatrix} \quad (3)$$

where \mathbf{A} is a symmetric $N \times N$ matrix, containing the values of the radial basis function, computed with the distance of the two corresponding control points, \mathbf{P} is a $N \times M$ matrix containing the polynomial extension, \mathbf{f} is a vector containing the data values and $\boldsymbol{\lambda}$ and $\boldsymbol{\gamma}$ are the weighting-vectors. After solving the system, the solution can be computed using Eq. (2) for each nodal point in the FE region.

Various different radial basis functions are available, where in this paper especially 4 different functions are considered

- linear RBF: $\phi = r$
- cubic RBF: $\phi = r^3$
- "thin-plate-spline" RBF: $\phi = r^2 \log r$
- multiquadratic RBF: $\phi = \sqrt{1 + (\epsilon r)^2}$

which are plotted in Figure 5. Subsequently, each point in the region can be approximated by evaluating Eq. (2).

The theory and also the implementation of this approach is rather simple and has been realized in the programming language Python. As will be discussed later, the approach leads to good results for the interpolation, depending on the ansatz of the polynomial augmentation and shows a rather stable behavior. Further information can for instance be obtained from [5] or [6].

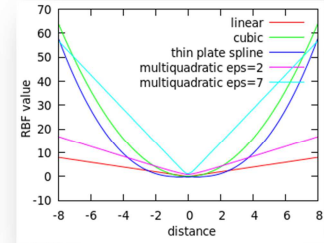


Figure 5: visualization of different radial basis functions

2.1.2 Kriging Approach

Kriging is a geostatistical technique, based on the minimization of a Lagrangian function to compute the weights λ_j in Eq. (1). The kriging equations are based on two conditions

1. minimization of the scattering of the estimation error, i.e.

$$\sigma_R^2 = Var [s^*(x) - s(x)] \rightarrow Min \quad (5)$$

where s^* denotes the kriging interpolation, s the real solution and $Var[...]$ the statistical variance of the difference, i.e. the estimation error.

2. match of the expected values (mean values $E[...]$), i.e.

$$E[s^*(X)] = E[s(X)] \quad (6)$$

which is also denoted as *unbiased condition*.

The latter condition (unbiased condition) performs a split of the function

$$u(X_i) = \psi_j(x) = c(X_i) + f(X_i) \quad (7)$$

into a drift function $c(X_i)$, representing the average behavior of $u(X_i)$ with $E[s^*(X)] = E[u(X)] = E[c(X)] = c(X)$ and a stationary fluctuation $f(X)$ with $E[f(X)] = 0$. Assuming polynomial functions $p_k(X)$ of degree M for the drift function this finally leads to the expression

$$p_k(X) = \sum_{i=1}^N \lambda_i p_k(X_i), \quad with \ k = 1, \dots, M \quad (8)$$

Using Lagrangian multipliers μ_k together with Eqs. (5) and (8), a Lagrangian can be formulated as follows

$$f(\lambda, \mu) = \sigma_R^2(\lambda) + \sum_{k=1}^M \mu_k \left(\sum_{i=1}^N \lambda_i p_k(X_i) - p_k(X) \right) \rightarrow MIN! \quad (9)$$

Deriving the function w.r.t. the unknowns (λ, μ) finally leads to the linear equation system

$$\begin{bmatrix} \mathbf{C} & \mathbf{P} \\ \mathbf{P}^T & \mathbf{0} \end{bmatrix} \begin{bmatrix} \boldsymbol{\lambda} \\ \boldsymbol{\mu} \end{bmatrix} = \begin{bmatrix} \mathbf{c} \\ \mathbf{p} \end{bmatrix} \quad (10)$$

where C_{ij} contains the covariance between the sample points X_i and X_j , while c_i contains the covariance between the sample point X_i and the evaluation point X . However, this equation system is not very useful since the right-hand-side also depends on the coordinates of the evaluation point and

the equation system has to be assembled and solved for each evaluation point which would be numerically very expensive. A further rearrangement of the equation system leads to a dual formulation, where the kriging matrix can be setup, depending on the choice and the initial coordinates of the control points. The right-hand-side only depends on the current coordinates of the control points and thus, the equations system can be solved in advance. The remaining nodes are then computed by a linear combination of the unknowns (λ, μ) . The derivation of the method can for instance be reviewed in [7] or [8].

2.2 Test Example

As a simple example to test the performance of the chosen interpolation procedures, a test box (Figure 6) is created, where 10 nodes on each side are fixed in space. Two nodes on the upper face are moved upwards in the vertical direction.

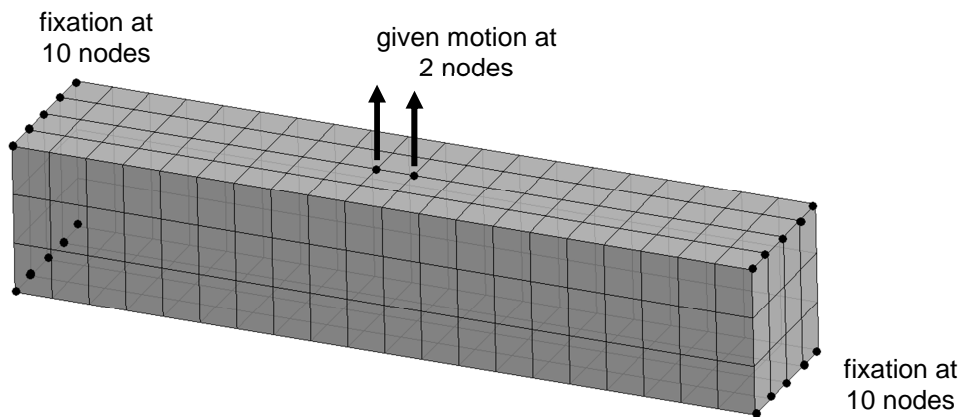


Figure 6: Simple test box, where 20 nodes are fixed and two nodes are moved upwards.

The results of the interpolation process using kriging and the radial basis functions are depicted in Figure 7 and Figure 8, where in the first case a constant polynomial extension was chosen, while in the second case a tri-linear extension was taken (linear in each spatial direction). The kriging approximation is the same for both cases and shows a good shape, the cross section is maintained and the shape is smoothly interpolated. The quality of the approximation highly depends on the choice of the radial basis functions and on the order of the polynomial extension. While the shapes in the first case (constant extension) show a very unsuccessful deformation state, the second case (tri-linear extension) shows a good match for all radial basis functions. The best approximation is however obtained using the cubic RBF approach, and closely matches the shape of the kriging approach.

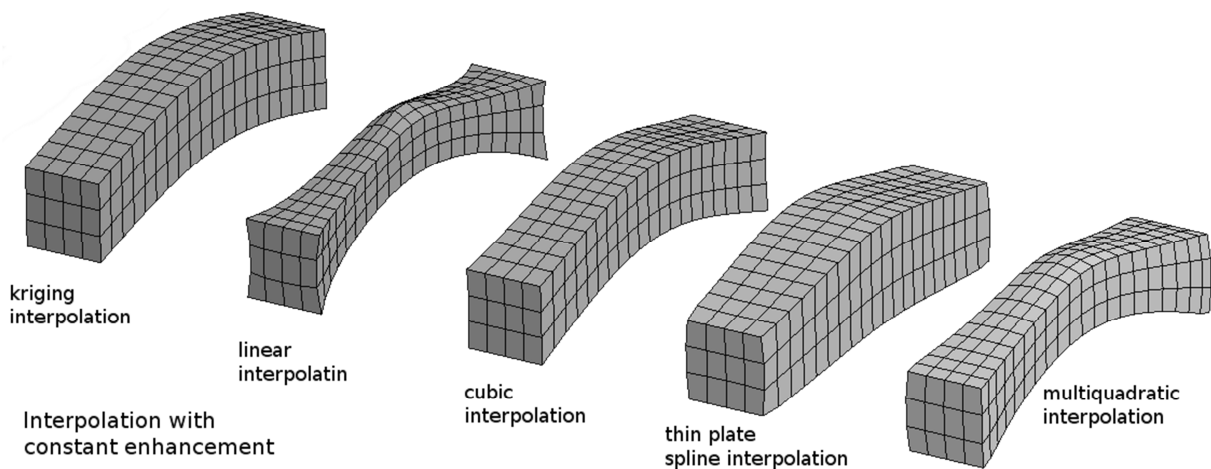


Figure 7: Results of the test box deformation using the kriging approach and the RBF approach with constant polynomial extension

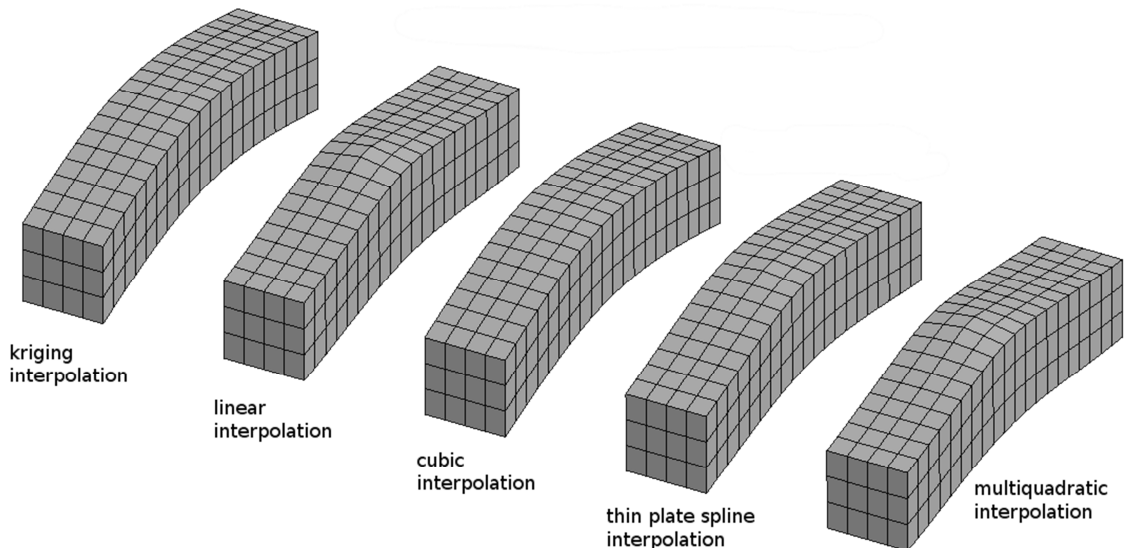


Figure 8: Results of the test box deformation using the kriging approach and the RBF approach with linear polynomial extension

3 Full Thorax Interpolation

In a first step, the whole thorax is interpolated in a single, holistic step. Landmarks, distributed on the rib cage, are chosen as the control points for the kriging/RBF interpolation. The destination landmarks are specific points on the rib cage geometry, obtained from CT scans. These landmarks are required to be well distributed to accurately describe the geometry of the destination thorax. For the adaptation of the FE model, the source landmarks have to be chosen on the FE rib cage geometry to match the destination landmarks as exactly as possible. The final geometry of the FE thorax heavily depends on the distribution and the matching of the landmarks. A bad landmark distribution or match might lead to strong geometric distortions, leading to a finite element mesh unusable for FE analyses. Thus, the choice of the landmarks is the crucial point for the full thorax interpolation process.

The advantages of a holistic approach are obvious. Depending on the landmarks, the whole thorax is adapted in a single step, where the interpolation functions and weights are computed from the motion of the landmarks. Any other node of the thorax can then be interpolated accordingly. This leads to a very fast and simple approach but due to the above mentioned problems, good shaped elements are difficult to obtain and ensure. A similar approach was used in [9] for the evaluation of different vulnerable populations in crash situations.

Figure 9 (left) shows an example landmark distribution on the bony thorax and the results of the interpolation of the THUMS thorax, based on the motion of the landmarks. Figure 10 illustrates some problems arising with this approach. Body parts can distort heavily and as a result, the FE mesh representation is not suitable for high-dynamic crash simulations. Another problem is the unphysical deformation of other body parts, which might be a side effect of badly distributed landmarks.

As a result, holistic interpolations of the whole geometry strongly depends on the input data and is therefore hardly suitable for finite element analyses, due to unrealistic deformations and bad element shapes.

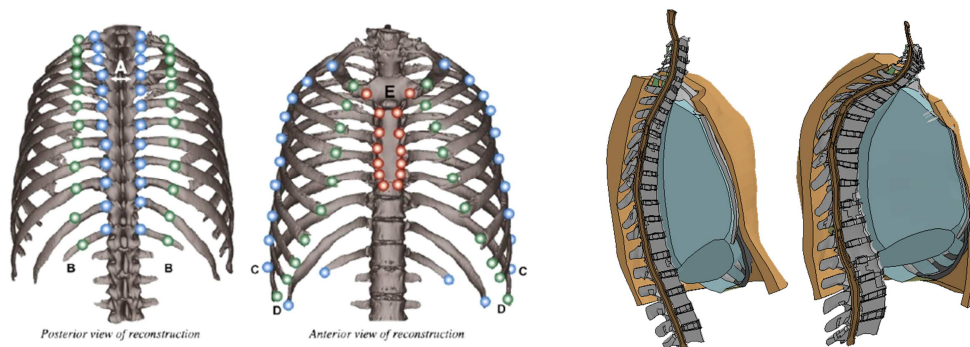


Figure 9: (left) example landmark distribution on the rib cage, (right) results of the holistic thorax interpolation with initial FE model and interpolated thorax model

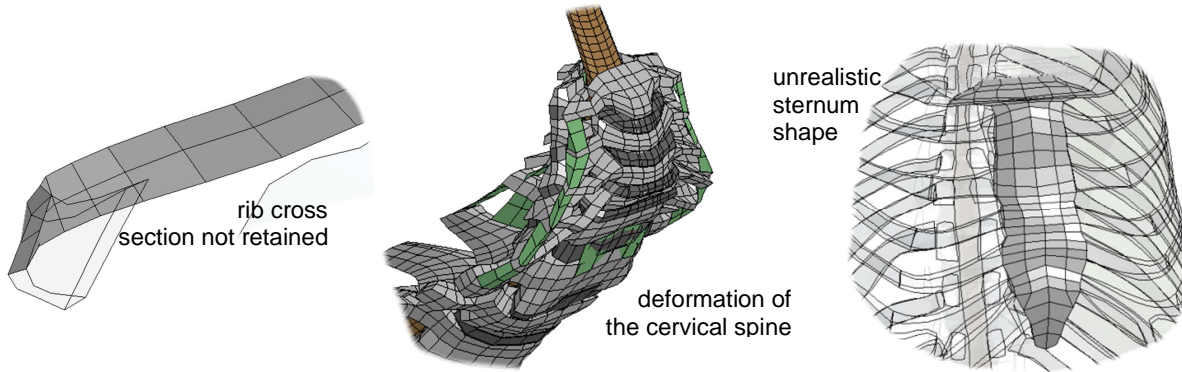


Figure 10: Illustration of some problems for the holistic interpolation (left) cross sections are not retained and might be heavily distorted, (center) strong distortions in the cervical spine area, (right) unrealistic deformation of parts, e.g. the sternum

4 Multistep Thorax Interpolation

For this reason, this section addresses an alternative multistep approach, where the geometry is adapted in multiple steps. This multistep approach is realized in terms of an input-based Python script, which is developed on the basis of the interpolation procedures, described earlier.

4.1 Development of an Interpolation Tool Box

This script is mainly based on an interpolation tool box, where various, simple and more complex geometric modification methods have been implemented which can optionally be combined with a smoothing step, based on nodal interpolations.

- ***MOVE** - move nodes and parts along a displacement vector. Optionally, a smoothing process can be active for a set of (transitional) parts.
- ***SCALE** - scale nodes and parts according to a reference node and local/global scaling factors. Optionally, a smoothing process can be active for a set of (transitional) parts.
- ***ALIGN/*ALIGN_CSYS** - align parts according to the motion of two reference points or the motion of a reference coordinate system, respectively. The parts to be aligned are not distorted but are rigidly relocated according to the reference.
- ***KRIGING_PARTS** - smooth (interpolate) parts with given boundary conditions. A pure smoothing step is performed, based on geometric changes from previous commands.
- ***PROJECT_NODES** - nodes can be projected to a given (shell) base part (compute local coordinates and distance to master shell) in the non-deformed geometry and reconstruct the nodal position in the deformed geometry. This ensures that cross sections are retained, even when the

```

-----
$ Step 4: project rib nodes
$
*PROJECT_NODES
TITLE, reconstruct rib nodes
$ define shell parts to be projected on
BASEPARTS, 8970200, 8970300
$ 8980200
$ define nodes to be projected/relocated
PROJPARTS, 8920000, 8920100, 8920200, 8920300, 8920400, 8920500, 8920600
PROJPARTS, 8920700, 8920800, 8920900, 8921000, 8921100, 8921200
PROJPARTS, 8922100, 8922200, 8922300, 8922400, 8922500, 8922600, 8922700
PROJPARTS, 8922800, 8922900, 8923000, 8924000, 8924100
PROJPARTS, 8923100,
$
*OUTPUT_FILE
out4-krig.k
$
-----
$ Step 5: fix skin/flesh
*KRIGING_PARTS
TITLE, fix skin/flesh parts
$ skin
KRIGPARTS, 8983000, 8983100, 8983200, 8983300, 8983400
$8370800,
$ outer costal pleura
KRIGPARTS, 8971000, 8971100
$ organs
KRIGPARTS, 8340020, 8940100, 8940200, 8950200
$ shoulder belt
KRIGPARTS, 8550100, 8550110, 8550500, 8550510
KRIGPARTS, 8650100, 8650110, 8650500, 8650510
$
$ rib base
CTRLPARTS, 8970200, 8970300, 8980200, 8971200, 8971300
$ inner costal pleura (Rippentfell)
CTRLPARTS, 8970000, 8970100
$
$
*OUTPUT_FILE
out5-krig.k
$
*KRIGING_PARTS
TITLE, abdomen area fix
KRIGPARTS, 8341100, 8341200, 8370000, 8370100, 8370900, 8370800
$8370120, 8370820, 8341010
$ spine
CTRLPARTS, 8330210, 8330310, 8330410
$ hip bone
CTRLPARTS, 8310112, 8310512
$
CTRLPARTS, 8983400
CTRLPARTS, 8340020
CTRLPARTS, 8370400
$
*KRIGING_PARTS
TITLE, neck area fix
KRIGPARTS, 8713000, 8713100, 8713200, 8713300
CTRLPARTS, 8880011, 8885011, 8880010, 8885010
CTRLPARTS, 8983300, 8983200
$
*OUTPUT_FILE
out6-krig.k

```

Figure 11: Batch script to adapt the thorax geometry using a sequence of geometric modifications

corresponding parts deform.

These geometric modification commands can be assembled in a batch script to adapt the geometry of the thorax as depicted in Figure 11. This batch script is then executed using the developed Python script and can easily be adapted to other requirements or geometric parameterizations.

4.2 Simplified Parameterization of the Thorax Adaptation

The adaptation process of the thorax still requires a geometric parameterization, i.e. a set of parameters which sufficiently describes the geometric changes. It was worked out in Section 3 that a parameterization using only the landmarks might be cumbersome and leads to different problems. In this paper, a simplified geometric parameterization is therefore used, which was derived from a CT scan database of various thoraces. The final shape of the rib cage is therefore given by only two parameters

1. *motion and deformation of the sternum* – motion vectors are defined to prescribe the final shape and position of the sternum relative to the initial thorax,
2. *thorax width in each rib plane* – to correct the lateral thorax shape, the width is given for each of the 10 rib planes.

It is furthermore assumed that the spine shape remains constant and is not deformed in the adaptation process. Although a very simple parameterization, these assumptions sufficiently describe the final shape of the FE thorax model.

Note that this is only an example parameterization of the geometric changes. Using the tool box, also other parameterizations can be easily incorporated.

4.3 Multi-Step Interpolation of the whole Body

Based on these assumptions, the final thorax geometry is obtained by 7 steps, which are described in the following in more detail. Generally, the assumptions are incorporated and the rest of the model is adapted to the new geometry using the general tool box.

Step 1: Adaptation of the Sternum Position and Shape

In the first step, the shape adaptation of the sternum is defined by displacements of various nodes on the sternum. The nodes are moved to their new position and an interpolation step is performed for the whole sternum. The results are depicted in Figure 12. Additionally, a comparison of the final shape for a kriging and a (cubic) RBF interpolation is shown, where the results are basically identical.

The adaptation is realized using a *MOVE command, where the $3 \times 6 = 18$ nodes of the sternum are moved to their final position. The nodes along the sternum define the correct shape while each displacement is tripled over the width to ensure the correct width of the sternum in each rib layer.



Figure 12: Results of step 1 – adaptation of the sternum (left) nodal motions of various sternum nodes and result, (right) comparison between kriging and cubic RBF interpolation

Step 2: Adaptation of the Rib Base

In the second step, the rib base – which is basically a shell part underneath the ribs and the sternum – and the inner costal pleura are adapted using an interpolation procedure. This is realized using the command `*KRIGING_PARTS`, where the parts of the rib base and the inner costal pleura are interpolated according to the motion of the sternum and the fixed spine. The results can be reviewed in Figure 13, where again the initial condition and the adapted shape of the second step is depicted (right). Again, the kriging and the (cubic) RBF interpolation approaches lead to very similar results and are thus not depicted here.

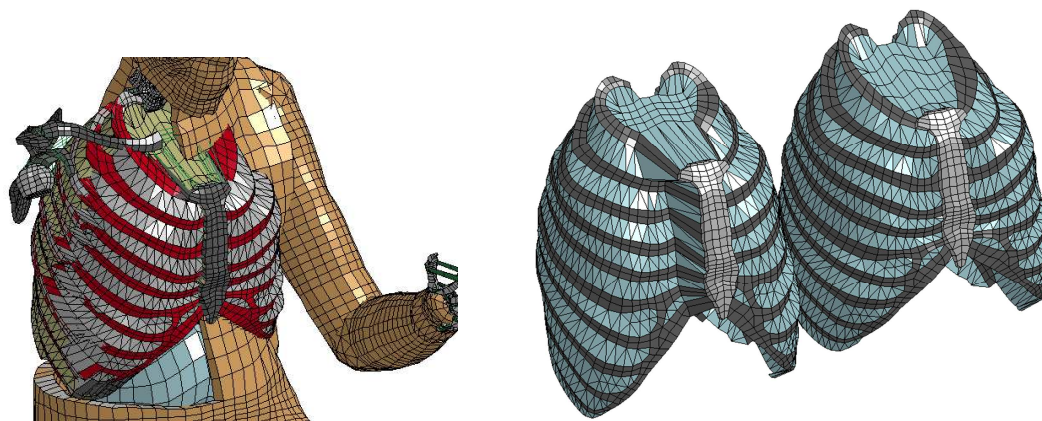


Figure 13: Results of step 2 – adaptation of the rib base and the inner costal pleura using an interpolation procedure

Step 3: Fix of the Thorax Width

The third step corrects the width of the thorax in each rib layer. Therefore the most lateral node of each rib is moved to match the measured thorax width and an interpolation approach is again applied using the new (moved) rib nodes, the sternum and the spine as control points. This is realized using the `*MOVE` command of the tool box. Figure 14 shows the results of the interpolation step.

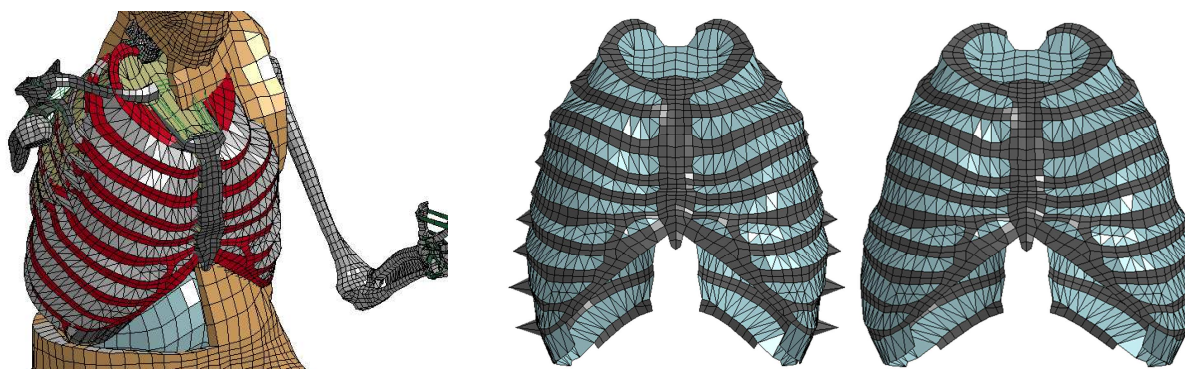


Figure 14: Results of step 3 – adaptation of the rib width (rib base) in each rib layer

Step 4: Reconstruction of the Ribs

The result of the first 3 steps is a new, adapted rib base. Step 4 performs a reconstruction of the rib geometry. In case of a pure interpolation approach for the whole ribs might lead to distorted ribs, where the rib cross sections are not retained. To avoid this, a projection-reconstruction step is performed using the command `*PROJECT_NODES`. The rib nodes are projected to the rib base, i.e. the closest shell element of the rib base for each rib node is evaluated and the local element coordinates and the distance to this shell element is computed on the initial geometry. The reconstruction process computes the new rib node coordinates, based on the current (deformed) rib

based. This approach minimizes the rib deformation and retains the cross section of each rib. The results are depicted in Figure 15.

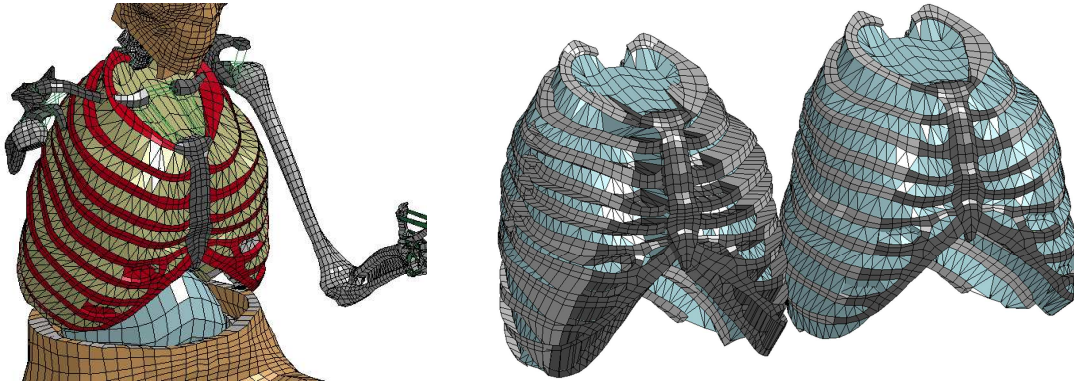


Figure 15: Results of step 4 – reconstruction of the ribs on the new rib base

Step 5: Adaptation of the thoracic Skin, Flesh and Organs

Based on the new rib cage, step 5 interpolates the rest of the thorax, i.e. the flesh, skin, organs and the shoulder belt. Control parts are the new ribs, the sternum and the (fixed) vertebrae. An interpolation approach is performed for the mentioned parts using the command *KRIGING_PARTS and the results are depicted in Figure 16.

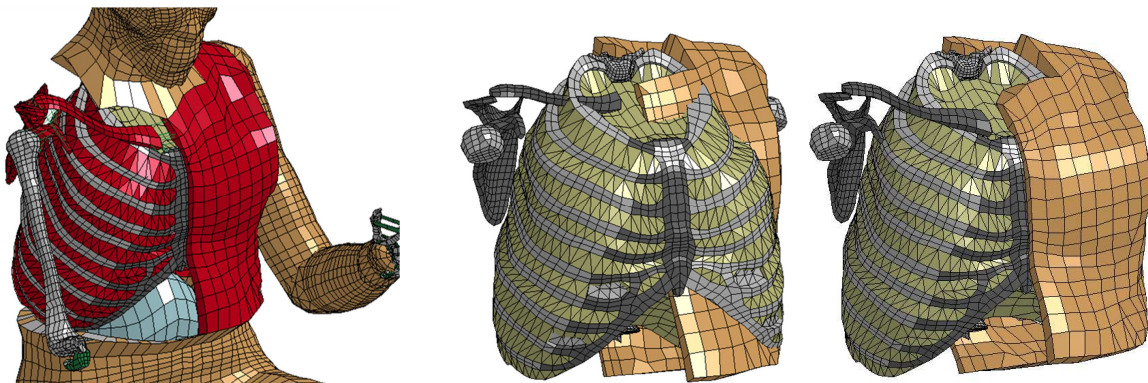


Figure 16: Results of step 5 – adaptation of the thorax (flesh, skin, organs and shoulder belt)

Step 6: Fix of the Transitions to the Head and the Abdomen

Based on the new geometry of the costal pleura and the thorax flesh, the neck and abdomen/pelvis area are interpolated using the command *KRIGING_PARTS. The result is depicted in Figure 17.

In summary, steps 1-6 can be performed automatically without interaction of the user. Different variants of the final shape can be easily accounted for by changing the input parameters (here: sternum position/shape and rib width). However, the setup of the adaptation sequence can be rather complex and requires some experience and trial-and-error. A different parameterization of the required thorax modification will most likely lead to a different sequence, where additional steps might be necessary and other steps have to be defined differently. After setting up the sequence, different variants can easily be incorporated.

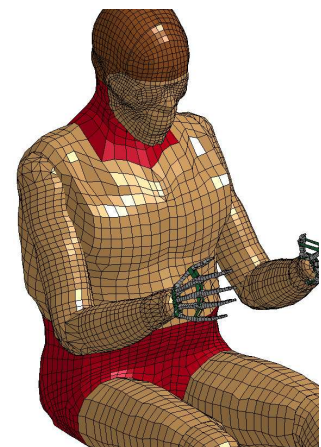


Figure 17: Adaptation of the transitional parts

Step 7: Remaining Model Fixes

It should be pointed out that the mesh quality after the first 6 (automatic) steps is very good and only a few manual fixes are still required. Therefore a 7th step is still necessary. This step mainly contains the following points

- *Merge of new nodal coordinates into the original model*
the previous 6 mesh modification steps only perform nodal relocations without changing the mesh connectivity. A merge of the new nodes into the original model ensures a consistent model after the adaptation process
- *Fix of extreme element distortions*
despite of the overall good model quality, single elements can still be heavily distorted after the smoothing process. These elements have to be identified and corrected manually
- *Fix of contact penetrations*
since contacts (tied and sliding contact) are not accounted for in the mesh adaption process, there will be most likely some contact penetrations in the new model. For stability reasons and to obtain a good mesh quality, these contact penetrations have to be identified and removed as far as possible

For the present problem, only less than 5 elements had to be corrected and about 7 contact penetrations had to be removed, which was performed using corresponding pre-processor and thus could be realized in a very short time.

The final results are depicted in Figure 18.

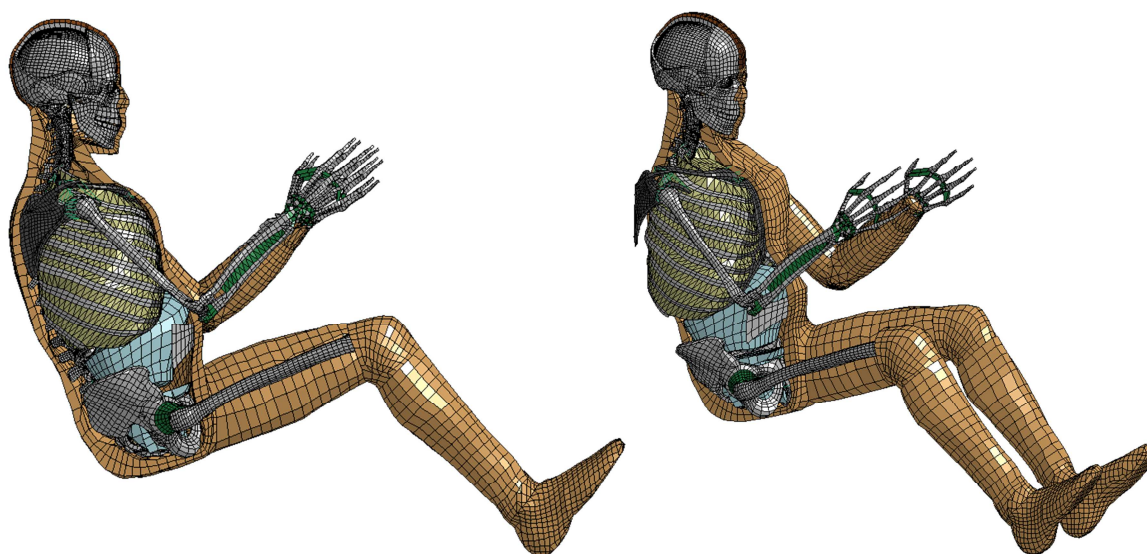


Figure 18: Final result of the thorax modification using the THUMS V3 occupant model

5 Summary and Outlook

This paper presented an automatic method to adapt the geometry of human body models to other body shapes. A holistic and a multi-step approach were discussed and drawbacks and advantages have been pointed out. Basic geometric transformation routines were implemented into a toolbox, realized in the programming language Python and two mesh smoothing procedures were defined, based on kriging and radial basis function interpolation. Finally, a Python script was developed to realize the geometric adaptation in a batch mode, where the commands from the geometric tool box can be arranged in a sequence to adapt the mesh accordingly.

Furthermore, a simplified parameterization was used for the adaptation of the thorax to the new geometry and the whole THUMSTM Version 3 model was adapted to the new geometry. This allows a very fast creation of different model variant and is thus also suitable for optimizations.

Future work on this approach might include a more sophisticated parameterization of the new thorax geometry. In this case, the final shape and position of the sternum and the chest width in each rib layer was used, already based on insights taken from a CT scan database. The approach might also be used to get more insights and define requirements on the distribution of the landmarks in a holistic interpolation approach, as described in Section 3. This approach represents a very simple way of interpolating the model geometry, without the need to define a complex sequence of different steps. One important feature would be the inclusion of automatic mesh checks and maybe mesh corrections to avoid heavily distorted elements and contact penetrations.

6 Literature

- [1] Fressmann, D et al: "FE Human Modelling in Crash – Aspects of the numerical Modelling and current Applications in the Automotive Industry", 6. LS-Dyna Anwenderforum, Frankenthal 2007
- [2] THUMS Information on the JSOL webpage, <http://ls-dyna.jsol.co.jp/en/thums/index.html>
- [3] THUMS Information on the DYNAmore webpage
http://www.dynamore.de/en/products/models/human?set_language=en
- [4] Global Human Body Models Consortium web page, <http://www.ghbmc.com>
- [5] Buhmann, M.D.: "Radial Basis Functions: Theory and Implementation", Cambridge University Press, ISBN 978-0-521-63338-3, 2003
- [6] Wright, G.B.: "Radial Basis Function Interpolation: Numerical and Analytical Developments", University of Colorado, 2003
- [7] Chaveesuk R., Smith A.E.: "Dual Kriging: An exploratory use in Economic Metamodeling", The Engineering Economist, 50:247-271, 2005
- [8] Trochu, F.: "A Contouring Program based on Dual Kriging Interpolation", Engineering with Computers, 9:160-177, 1993
- [9] Hu J., Rupp J.D., Reed M.P.: "Focusing on Vulnerable Populations in Crashes: Recent Advances in Finite Element Human Models for Injury Biomechanics Research", Journal for Automotive Safety and Energy, 2012, Vol 3, No 4.